Dust formation and transport in very low-pressure ECR acetylene plasma

M. Rojo[1, 2], X. Glad[1, 2], J.L. Briançon[3], S. Dap[1], J. Margot[2], R. Clergereaux[1]

[1]LAboratoire PLAsma et Conversion d'Energie, Université Paul Sabatier, Toulouse, France
[2]Laboratoire de physique des plasmas, Département de physique, Université de Montréal, Montréal, Québec, Canada
[3]Institut Jean Lamour, Université de Lorraine, Nancy, France

Abstract: In this work, the formation and transport of carbonaceous dust particles are studied in an acetylene ECR plasma using fast imaging of dust particles along with ex-situ analysis of collected matter. It seems that both volume and surface mechanisms are involved in the particles formation. Moreover, the dynamics of dust particles exhibits particular trends and strongly influences the physical mechanisms arising in particles formation.

Keywords: ECR, magnetized plasma, dusty plasma, transport.

1. Introduction

Dust particles formation is observed in different kind of plasmas such as interstellar and circumstellar environments [1], reactive low-temperature laboratory plasmas [2], or during plasma-surface interaction in Tokamaks [3]. Inside fusion devices, plasma-surface interactions lead to a significant amount of dust. Once reemitted inside the plasma volume, they affect the plasma properties [4] (density, temperature), the performances of the device and lead to safety issues [5]. In this context the formation and dynamics of dust need to be well understood. The harsh plasma environment heats the dust and makes them incandescent. A solution to obtain a direct image of dust dynamics is to track them with fast imaging [6]. This technique allows to reconstruct dust trajectories in two or three dimensions, determining their instantaneous velocities and accelerations, hence describing the forces applied on them.

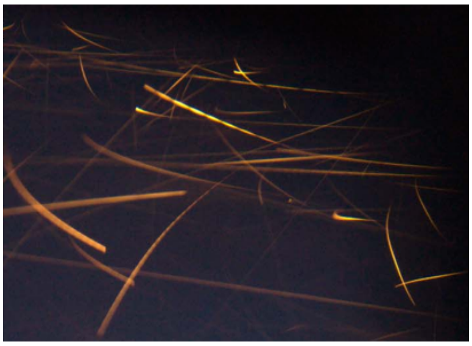

Fig. 1. Naked-eye observation of incandescent dust particles produced in a pure acetylene electron cyclotron resonance excited plasma [7].

Recently in LAPLACE, we observe the outbreak of incandescent dust particles as shown in Fig. 1, inside an electronic cyclotron resonance (ECR) plasma device [7]. In agreement with fusion devices, the incandescence of dust particles could be related to the characteristics of the ECR plasma (high densities and very energetic primaries electrons). In the present study, mechanisms of formation and dynamics of dust particles produced in an ECR plasma are studied using fast imaging, ex-situ analyses and Langmuir probe measurements.

2. Experimental setup

a. Linear ECR plasma reactor.

The experimental setup is presented in Fig. 2. The linear ECR plasma reactor consists of a parallelepiped stainless steel tank. Underneath is placed a "racetrack" Samarium-Cobalt magnet, with a magnetic surface intensity of 3300 Gauss (central and external magnets have opposite polarities). The ECR heating is produced by a microwave (MW) linear antenna located above one of the external magnet, underneath the 875 Gauss iso-line. We call magnetic cusps the zone where the magnetic field lines converge above the magnetic poles. Also, we call plasma lobes the areas between the magnets where charged species are trapped by the magnetic field. For all experiments the generator delivers an injected power of 200 W. The gas inlet is located on the side above the antenna and the gas outlet on the opposite side. The plasma is produced with 0.6 mTorr of pure acetylene.

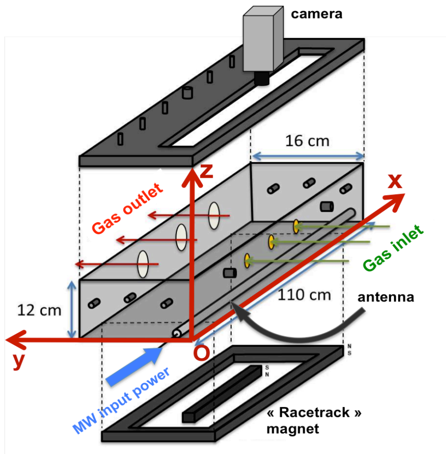

Fig. 2. Linear ECR apparatus sketch.

We impose an Oxyz coordinate system where the origin is at the closest corner to the MW input. The positioning of the axis is important as all the velocities, accelerations components are related to them. On the top, a long glass window allows us to film dust particles with the fast camera between the central and external magnet in the Oxy plane. A typical experiment lasts one hour and consists in filming incandescent dust at one position at different times. This experiment is repeated at different positions.

b. Tracking procedure.

The tracking of incandescent dust is realized with the TRAcking and Classification of pin-point Event algorithm (TRACE) [8]. TRACE returns a table containing dusts positions, light intensities, and apparent surfaces for each image. We use a Photron APX-RS that allows us to film the particles at 20 000 fps. Each film lasts one second. The resolution associated with that velocity is 384x256 pixels (being a window of 1.7x2.5 cm). The height where most dust particles are detected is $z \approx 3$ cm and the lens depth of field is nearly 1 mm. We use some specific tracking parameter to ensure the tracking accuracy. A dust cannot be detected if (1) it crosses more than 20 pixels between two frames (it is not possible to detect the particle position precisely beyond) and (2) the diameter of apparent surface is more than 15 pixels (dust surfaces increase when they are leaving the focal plane). In addition, we check the accuracy of the detection process by comparing reconstructed dust trajectories with the original movie. With this procedure we estimate to detect nearly 30% of all dust in a film.

We remind the reader the tracking with one camera

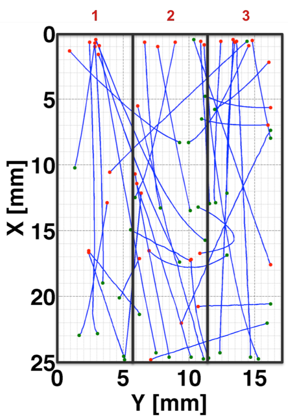

Fig. 3. Example of reconstructed incandescent dust trajectories (0.6 mTorr pure acetylene plasma at t = 12 min). A movie analysis can be divided into three columns.

allows us a 2D description of dust dynamics (in the Oxy plan at z=3cm, between the external and central magnets). Once the table is generated by TRACE, we use it to have a direct access to each particle velocities, accelerations at different times and positions. An example of TRACE analysis is shown in Fig.3. Note that the analysis can be performed on three different columns, as schematized in Fig. 3, allowing comparative studies of the particles transport along the Y-axis.

3. Kinetic dust apparition

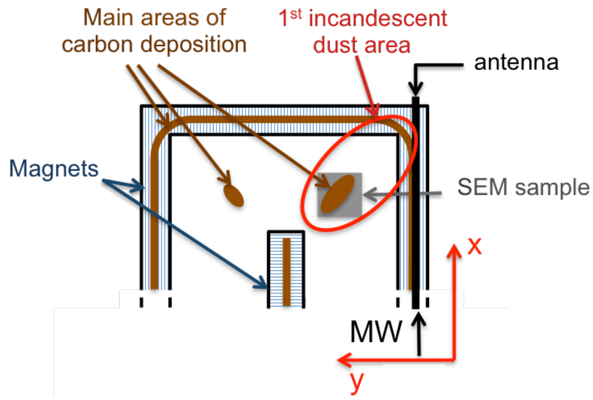

Fig. 4. Sketch of the reactor focused on the magnetic corner away form the MW injection and showing the main areas of carbon deposits (brown lines and spots). The area where the 1st incandescent dust particles are observed (red oval) is also highlighted.

In the following part part we focus on the temporal evolution of dust particles. The Fig. 4 represents a sketch of two magnetic corners opposite to the MW injection. It shows the main areas of carbon deposition: on the magnetic cusp and in the magnetic turns. The red delimited area represents where the first incandescent dust particles appear. The specificity of the right spot of carbon deposition is that it also starts being incandescent after 10 minutes. We call the incandescent spot the “hot spot” (HS).

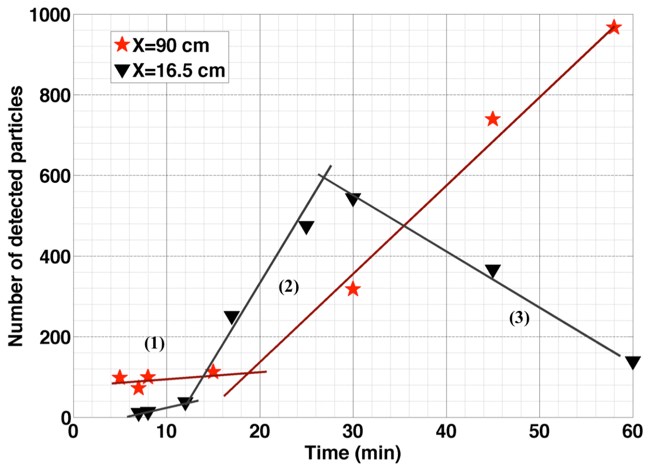

Fig. 5. Temporal evolution of the particles numbers detected. Red stars and black triangles are related to the position, respectively x = 90 cm and x = 16.5 cm. Lines are plotted to highlight the tendencies

Fig. 5 depicts the temporal evolution of dust particles detected by TRACE at two distinct positions: x = 16.5cm (black lines and triangles) and x = 90 cm (red lines and stars). For the sake of clarity, we choose to show only two positions. First, in both cases, we notice the absence of incandescent dust in the first minutes. After 5 minutes, (1) the number of detected particles increases weakly (with a rate constant of 5 particles per minute) until approximately 15 minutes. Then, (2) it sharply increases with a rate constant 6 times higher. In some cases, (3) a decrease of dust particles apparition occurs.

To characterise the plasma surface interactions, stainless steel samples were positioned on the HS. Samples were exposed to the plasma for different times: 1 (no incandescence of the HS), 7 (incandescence starts) and 10 minutes (bright orange incandescence). Samples are analysed by Scanning Electron Microscopy (SEM – JEOL JSM 6700F) as reported on fig. 6. On the first two samples (Fig. 5.a and b), the deposit consists in 10 nm carbon spherical nanoparticles. For a longer duration, they agglomerate into a smoother deposit (Fig. 5.c), which could be explained by a local heating due to high charged particles fluxes [9]. Eventually, the deposit seems to delaminate forming few tens of μm flakes that should be ejected in the plasma volume (Fig. 5.d). This phenomenon is similar to plasma-surface interactions reported in fusion devices [10].

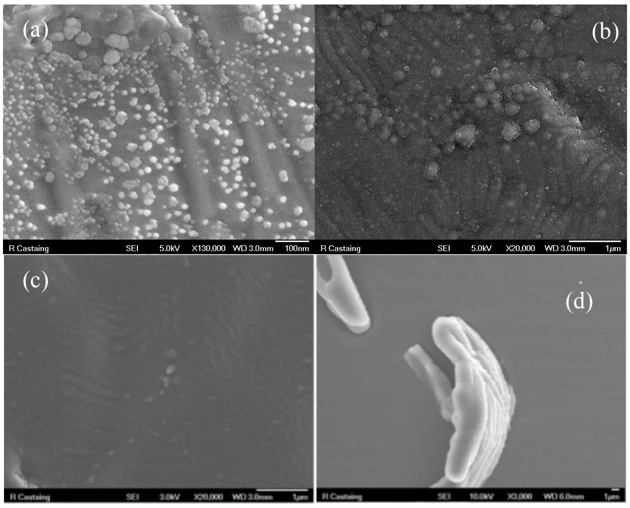

Fig. 6. “Hot Spot” SEM images for different exposure times: (a) 1, (b) 7, (c) 10 and (d) 60 minutes.

The spherical shape of nanoparticles presented in fig. 6 (a) shows that the first dust particles are formed inside the plasma volume. It also shows that all the particles are not necessarily incandescent. Else we would detect more and particles and not only at $z \approx 3$ cm. The carbon nature could play a significant role in the dust incandescence.

The transition between the regimes (1) and (2) seems to be correlated with plasma-surface interactions. In the first 15 minutes, dust particles are preferentially deposited on the magnetic cusps and the HS. In regime (2), the deposit on the HS starts being incandescent, probably leading to a process of remobilization explaining the high detection rate of incandescent particles. The regime (3) is not yet fully understood and only speculation can be advanced. We suggest that less carbonaceous matter is remobilized in the plasma volume, leading to a decrease of the particles detected. This could have to do with the thickness of the deposit preventing its delamination or a dehydrogenation of the latter and further crystallization of the carbon due to thermal effects.

4. Dust particles dynamics

To help understand the incandescent dust transport, fast imaging has been performed at eight different positions along the X-axis after 45 minutes. Fig. 7 (a), (b) and (c) represent the distribution of the X component of the acceleration respectively at x = 90, x = 62.5 and x = 12.5 cm. Fig. 7 (d) shows the mean acceleration (of the X component) of all the particles detected in a movie at 8 different positions. For $0 < x < 50$ cm, the particles are mainly transported toward the microwave input (fig. 7(c)). We observe an opposite behaviour at $80 < x < 100$ cm, the particles are transported toward the opposite side of the reactor (fig. 7(a)). In between, the average X component of acceleration tends toward zero (fig. 7(b)). As reported on fig. 7 (d), the average X component of the acceleration increases quite monotonously with the X position. It suggests that the force able to transport the incandescent dust particles changes direction along the X-axis.

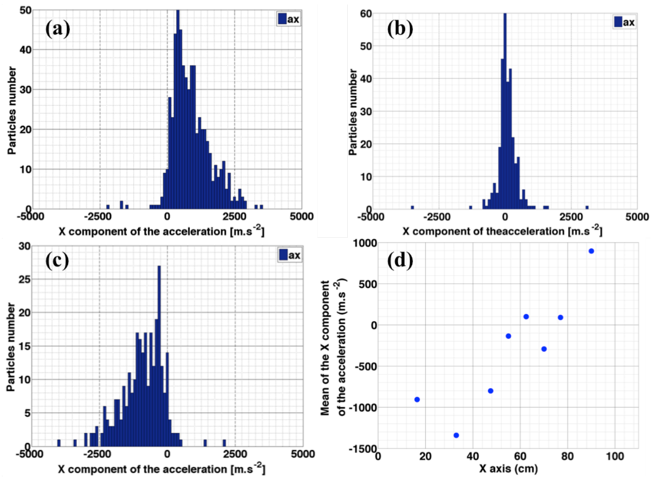

Fig. 7. Distributions of the X component of the acceleration after 45 for different positions: (a) x = 90, (b) x = 62.5, (c) x = 16.5 cm. Fig. 7 (d) represents the average of the X component of the acceleration along the X-axis.

It is difficult to conclude on the main forces acting on dust particles in the X-direction. Two can retain our attention: electric and ion drag forces. The electric field along the X-axis was determined by Langmuir probe measurements in argon plasma at 1 mTorr. The plasma potential profile is reported in Fig. 8. It does not show any potential gradient inversion: in this case, the electric field is independent of the X-position and constant with a value of about 4 $V.m^{-1}$. The electrical force alone cannot be responsible of dust transport. We know after [9] that high ion fluxes are measured on the magnetic cusps and on the HS where we observe the first nanoparticles deposition. Hence, ion drag force could also play a role on the X-axis transport. Ion drag along the X-axis could be related to E×B, ∇B×B or diamagnetic drift. The E×B drift implies the inversion of the electrical field on the Z-axis. This observation has not been made in argon plasma at 1 mTorr. Also the ∇B×B drift cannot explain the transport inversion along the X-axis because of the linear geometry of the "racetrack" magnet.

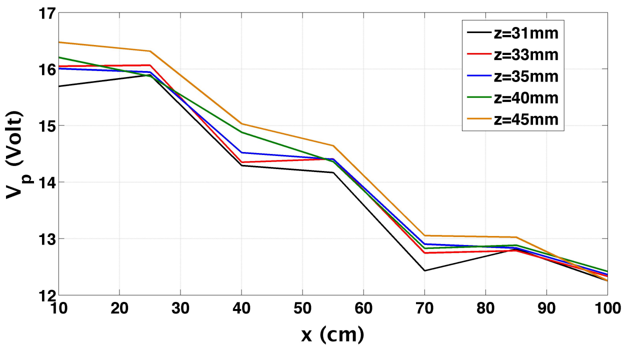

Fig. 8. Plasma potential profile along the X-axis in pure argon plasma at 1 mTorr.

Now we focus on the Y-axis direction. Along this direction, the distribution of the Y component of the acceleration obtained on the whole picture was found to be quite symmetric and centred on zero. Hence a more accurate analysis was performed splitting the picture in to three columns (Fig. 9).

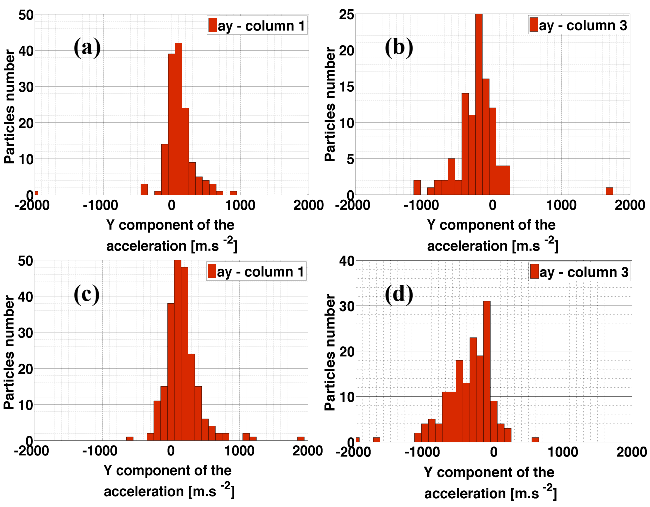

Fig. 9. Distributions of the Y component of the acceleration after 45 minutes for different positions and different columns: (a) x = 16.5 cm (column 1), (b) x = 16.5 cm (column 3), (c) x = 90 cm (column 1) and (d) x = 90 cm (column 3).

In the first column (fig. 9 (a) & (c)), the distributions are oriented toward positive values of acceleration. While in the third column (fig. 9 (b) & (d)) the distributions are oriented toward negative values. Hence a force is constantly attracting dust in the middle of the plasma lobes. If we assume negatively charged dust (despite their incandescence), we suggest they could be accelerated by an electric field along the magnetic field line [11].

5. Conclusion.

In this work we studied the formation and dynamics of incandescent dusts particles. We used fast video imaging, Langmuir probe measurements, and observations of matter collected at the "Hot Spot" with SEM.

We have shown in this work that the reactor is first filled with 10 - 30 nm spherical carbonaceous particles. Those particles deposit on specific area of the reactor (HS and magnetic cusp) to form a smooth film. Due to plasma-surface interaction, a heating mechanism erodes the film on the HS area. We suggest fragments of carbonaceous material are reemitted in the plasma volume. The incandescence of dust particles could be related to the characteristics of the ECR plasma (very energetic primaries electrons) and the carbon nature (amorphous, hydrogenated, graphitic).

Additionally, we have carried out a dust transport study along the X and Y-axes. We obtained the accelerations tendencies and showed that a force tends to confine dust in the centre of the plasma lobes (Y-axis transport) and another one tends to push them to each extremities of the reactor (X-axis transport). Finally, we showed that the electrical force alone could not explain the transport along the X-axis.

6. References

[1] Henning, T., & Salama, F. *Science*, *282*(5397), 2204-2210. (1998).

[2] Deschenaux, C., Affolter, A., Magni, D., Hollenstein, C., & Fayet, P. *Journal of Physics D: Applied Physics*, *32*(15), 1876. (1999).

[3] Winter, J. *Plasma physics and controlled fusion*, *40*(6), 1201. (1998).

[4] Winter, J. *Plasma physics and controlled fusion*, *46*(12B), B583. (2004).

[5] Sharpe, J. P., Petti, D. A., & Bartels, H. W. *Fusion Engineering and Design*, *63*, 153-163. (2002).

[6] Brochard, F., Shalpegin, A., Bardin, S., Lunt, T., Rohde, V., Briançon, J. L., ... & Neu, R. *Nuclear Fusion*, *57*(3), 036002. (2016).

[7] Drenik, A., Yuryev, P., & Clergereaux, R. *IEEE Transactions on Plasma Science*, *39*(11), 2734-2735. (2011).

[8] Brochard, F., Shalpegin, A., Bardin, S., Lunt, T., Rohde, V., Briançon, J. L., ... & Neu, R. *Nuclear Fusion*, 57(3), 036002. (2016).

[9] Glad, X., Gaboriau, F., Rojo M., Dap, S. & Clergereaux R., *ISPC 23 proceeding* (2017).

[10] De Temmerman, G., Bacharis, M, Dowling, J & Lsigo S. *Nuclear Fusion*, 50(10), 105012 (2016).

[11] Lagarde, T., *Study of plasma production and diffusion in sources excited by distributed electron cyclotron resonance* (PhD thesis). Chapter 2. Université de Grenoble (1994).